Title

Understanding of electrochemical K+/Na+ exchange mechanisms in layered oxides

Authors

Kim, Haegyeom

Byeon, Young-Woon

Wang, Jingyang

et al.

Publication Date

2022-05-01

DOI

10.1016/j.ensm.2022.01.057

Peer reviewed

Energy Storage Materials 47 (2022) 105–112

Contents lists available at ScienceDirect

Energy Storage Materials

journal homepage: www.elsevier.com/locate/ensm

Understanding of electrochemical K^+/Na^+ exchange mechanisms in layered oxides

Haegyeom Kim [a,*], Young-Woon Byeon [a], Jingyang Wang [b], Yaqian Zhang [b], Mary C. Scott [b], KyuJung Jun [a,b], Zijian Cai [a,b], Yingzhi Sun [a,b]

[a] Materials Sciences Division, Lawrence Berkeley National Laboratory, Berkeley, CA 94720, United States
[b] Department of Materials Science and Engineering, University of California, Berkeley, CA 94720, United States

ARTICLE INFO

Keywords:
Ion-exchange
Layered oxides
Cathode
Batteries
Sodium
Potassium

ABSTRACT

Ion-exchange reactions are commonly used to develop novel metastable electrode materials for alkali-ion batteries that cannot be synthesized using direct chemical reactions. In this study, the electrochemical K to Na ion-exchange reaction mechanisms in a layered K_xCoO_2 cathode as a model system were investigated using *operando* and *ex situ* structure characterization techniques. Some level of K ions was observed to remain in the layered structure during the electrochemical ion-exchange reactions. Interestingly, the K ions are well separated from the Na-rich phases in the discharged state, and they form an intermediate phase in which K and Na ions are mixed at the top of charge. We discovered that such residual K ions prevent the collapse of the layered structure in the high-voltage regime, thereby improving the cycling stability in a Na-battery system.

1. Introduction

The ion-exchange reaction is ubiquitous and is used to produce a wide variety of materials, including clays, zeolites, oxides, and phosphates [1]. The ion-exchange reaction is also an important synthetic method for the synthesis of metastable materials that cannot be obtained by direct chemical reactions such as conventional solid-state methods. In the ion-exchange reaction, a mobile ion is extracted from the host structure, with the insertion of another ion species, forming a novel compound. Ion-exchange reactions have been widely used in the development of novel electrode materials for alkali-ion batteries. For example, although O3-type $LiCoO_2$ is the most stable phase thermodynamically, the metastable O2-type $LiCoO_2$ can be synthesized via ion-exchange reaction from P2-type $Na_{0.7}CoO_2$ [2]. Layered $LiMnO_2$ was also first synthesized via the Na^+/Li^+ exchange reaction [3,4]. Since then, significant efforts have been devoted to the development of novel Li cathode materials using ion-exchange reactions, through which structural features of Na layered oxides can be adopted [5–7]. Eum et al. developed O2-type $Li_x(Li_{0.2}Ni_{0.2}Mn_{0.6})O_2$ by ion-exchange reaction from its Na analogue and demonstrated that the cation migration becomes more reversible in the O2-type structure than in the O3-type structure, thereby enabling significant reduction of the voltage decay [8]. Similarly, Xin et al. and Yang et al. synthesized Li-excess O2-type $Li_{0.66}[Li_{0.12}Ni_{0.15}Mn_{0.73}]O_2$ and $Li_x[Li_{0.2}Mn_{0.8}]O_2$ cathodes via Na^+/Li^+ exchange reaction, both of which exhibit suppressed layer-to-spinel phase transition and lattice oxygen loss during the charging [9,10].

Recently, new electrode materials for beyond Li-ion batteries have also been developed using ion-exchange reactions. P2-type $K_{0.5}CoO_2$ was successfully synthesized from P2-type $Na_{0.84}CoO_2$ [11,12]. In addition, P3-type K_xCrO_2 ($x < 1.0$) synthesized via ion-exchange reaction from $NaCrO_2$ has been proposed as a potential cathode material for K-ion batteries [13]. Our group also developed a novel compound $K_{1.66}Na_1Ni_2SbO_6$ via Na^+/K^+ exchange reaction [14]. A recent work by Nathan et al. demonstrated that ion-exchanged P2-type $K_{0.62}Na_{0.08}[Cr_{0.85}Sb_{0.15}]O_2$ undergoes a smaller lattice change during the charging–discharging process and improves cycling stability when compared with P2-$K_{0.7}[Cr_{0.85}Sb_{0.15}]O_2$ [15]. Na^+/K^+ exchange is not just limited to layered oxide cathodes but has also been applied to polyanion-type cathode materials for K-ion batteries [16–18]. It has also been demonstrated that the ion-exchange method is a powerful tool to develop novel cathode materials for multivalent-ion batteries, including Zn-ion and Ca-ion batteries [19–23].

The mechanisms of solid-state ion-exchange reaction are not yet fully understood and require further investigation. The ion-exchange reaction has been described as a continuous inter-diffusion of two distinct ions in the solid state, which is driven by their concentration gradient, or more precisely their chemical potential difference [1]. However, recent studies have revealed that the ion-exchange reaction appears to involve

* Corresponding author.
E-mail address: haegyumkim@lbl.gov (H. Kim).

https://doi.org/10.1016/j.ensm.2022.01.057
Received 12 October 2021; Received in revised form 5 January 2022; Accepted 30 January 2022
Available online 2 February 2022

a more complex process. For example, a phase separation between Li- and Na-rich domains during Na^+/Li^+ exchange has been identified in X-ray diffraction (XRD) studies by several groups [6,24-26]. Transmission electron microscopy (TEM) and electron backscatter diffraction (EBSD) studies have also confirmed that Na-rich domains are segregated from Li-rich domains when the Na ion is electrochemically exchanged with Li in $Li_xNi_{1/3}Mn_{1/3}Co_{1/3}O_2$ and Li_xCoO_2 [25,27]. Similarly, Na- and K-rich phases have been simultaneously observed during electrochemical Na^+/K^+ exchange reaction in Na-layered oxides using XRD and TEM [11,14].

As part of our continuing efforts to better understand ion-exchange reaction mechanisms, in this study, we investigated the K^+-to-Na^+ exchange reaction process in a P2-type K_xCoO_2 model system. The electrochemical ion-exchange method offers several advantages: (i) it is easy to control the rate of ion-exchange reaction using a potentiostat in galvanostatic mode, (ii) sequential reaction enables easy identification of intermediate phases, and (iii) it can overcome thermodynamic or kinetic barriers that often appear in chemical ion exchange. Our XRD characterization showed that K-rich and intermediate (likely K/Na mixed) phases form during the K^+/Na^+ exchange reaction in K_xCoO_2. Unlike the ion exchange from Na^+ to K^+ [14], in the reverse direction, K and Na ions are widely distributed within a particle during the K^+-to-Na^+ exchange case, as confirmed using the TEM energy-dispersive spectroscopy (EDS) mapping technique. We also found that some residual K ions remained even after several electrochemical K^+/Na^+ exchange cycles, which might explain the improved cycling stability of K_xCoO_2 in a Na cell due to the pillar effect of large K ions, as suggested in a recent work from Wang et al. [28].

2. Experimental section

2.1. Materials synthesis

The P2-type K_xCoO_2 ($x = 0.6$) was synthesized using a solid-state method. An excess amount (9 at%) of K_2CO_3 (>99%, Sigma-Aldrich) was homogeneously mixed with Co_3O_4 (<10 μm, Sigma-Aldrich) using a planetary ball mill (Retsch PM200) at 300 rpm for 4 h. The resulting mixture was pelletized and fired at 700 °C for 50 h under a flowing O2 environment. After natural cooling, the temperature was held at 200 °C before the samples were collected to prevent contamination from moisture in the air. For the synthesis of P2-type Na_xCoO_2 ($x = 0.74$), an excess amount (4 at%) of Na_2CO_3 (>99%, Sigma-Aldrich) was homogeneously mixed with Co_3O_4 (<10 μm, Sigma-Aldrich), and the other processes were conducted under the same conditions for K_xCoO_2 synthesis.

2.2. Characterization

The crystal structures of the obtained materials were analyzed using XRD (Rigaku Miniflex 600) with Cu Kα radiation. Operando XRD was performed on a Bruker D8 Advance X-ray diffractometer using Mo Kα radiation. A homemade operando cell with a Be window was galvanostatically cycled at 2 mA g^{-1} between 1.6 and 4.15 V using a Maccor potentiostat, and XRD patterns were collected from 5° to 35° 2θ every 40 min at room temperature. The particle morphology was verified using field-emission scanning electron microscopy (FE-SEM; Zeiss Gemini Ultra-55). The HAADF-STEM and EDS maps were collected on a FEI TitanX 60–300 microscope equipped with a Bruker windowless EDX detector at an acceleration voltage of 300 kV. The K_xCoO_2 electrode was dissembled from the cell after the first charge and first charge–discharge cycle. The cycled K_xCoO_2 electrodes were then dispersed into anhydrous diethyl carbonate (DEC) and sonicated to obtain good particle dispersion. The TEM samples were prepared by depositing a drop of dilute K_xCoO_2 dispersion onto a TEM grid with a lacey carbon support and allowing the solvent to evaporate at room temperature in an Ar-filled glovebox. The samples were loaded into a Gatan 648 vacuum-transfer holder to transfer the sample from the glovebox to the microscope without air exposure. Air-free X-ray photoelectron spectroscopy (XPS) measurements were performed on a Thermo-Fisher K-Alpha Plus XPS/UPS with a monochromatic Al X-Ray source (1.486 eV) at the Molecular Foundry at Lawrence Berkeley National Laboratory. The sample films were transferred into the XPS system using a Thermo-Fisher K-Alpha Vacuum Transfer Module to avoid air exposure. The spectra was acquired with passing energy of 50 eV and a dwell time of 50 ms. X-ray absorption spectroscopy (XAS) measurements at Co K-edge were performed in a transition mode at Beamline 20-BM-B of the Advanced Photon Source, Argonne National Laboratory. A Si (111) monochromator was used for selecting the incident beam energy. Normalization and calibration of raw data were carried out by Athena software [29]. A Rh-coated mirror was applied to get harmonic rejection. The samples for XAS analysis are prepared in film forms.

2.3. Electrochemical tests

The cathodes were prepared by mixing K_xCoO_2 (70 wt%), Super P carbon (Timcal, 20 wt%), and polytetrafluoroethylene binder (DuPont, 10 wt%) in an Ar-filled glovebox. Cathodes with a loading density of ~3.2 mg cm^{-2} were assembled in a two-electrode configuration using a Na-metal anode and glass-fiber separator (Whatman, GF/F) in a 2032 coin cell. The electrolyte was custom-made using 1 M $NaPF_6$ (American element) in anhydrous ethylene carbonate/diethyl carbonate (EC/DEC) (1:1 by volume, TCI America). Electrochemical tests were performed on a battery testing station (Arbin Instruments) at room temperature in galvanostatic mode. The electrochemical charge–discharge cycling was performed between 4.1 and 1.7 V at 3 mA g^{-1}.

2.4. Computations

Density functional theory (DFT) calculations were performed within the projector augmented wave (PAW) formalism [30] to compute the ion exchange reactions in P2-type $(Na/K)_xCoO_2$ materials, as implemented in the Vienna ab initio simulation package (VASP) [31]. A supercell size of 2 × 2 × 1 with 16 oxygen atoms was used, and 9 distinct alkali metal concentrations were computed from $x = 0$ to $x = 1$. For each alkali metal concentration, the lowest 10 alkali-metal-vacancy orderings ranked by Ewald energy were selected using Pymatgen software [32] and their total energies were computed in DFT. For the total energy calculations in DFT, full relaxations were performed to allow the geometry optimization with force convergence criteria of 0.01 eV/Å on all atoms and energy convergence criteria of 10^{-5} eV. A mixed scheme of the generalized gradient approximation (GGA) and GGA with Hubbard (+U) correction [33] was employed to compute the reaction energies.

3. Results

3.1. Electrochemical K- to Na-ion exchange in k_xCoO_2

To investigate the electrochemical ion-exchange reaction mechanisms, we first synthesized P2-type K_xCoO_2 ($x = 0.6$) as a model system using a conventional solid-state method. Fig. 1a presents the XRD pattern of the synthesized K_xCoO_2, which matches well with the simulated one. The small peaks at 33–34° are likely due to the impurity of KOH. A scanning electron microscope (SEM) image of P2-type K_xCoO_2 is presented in the inset of Fig. 1a, showing a large particle size of ~20–30 μm. Fig. 1b presents the charge–discharge profiles of P2-type K_xCoO_2 in a Na-half cell, where 1 M $NaPF_6$ in EC/DEC and Na metal are used as the electrolyte and counter electrode, respectively. The capacity of the first charge process is ~60 mAh g^{-1}, and the following charge and discharge capacity is ~110 mAh g^{-1} at 3 mA g^{-1}. Overall, the charge–discharge profiles are similar to those of P2-type Na_xCoO_2 ($x = 0.74$), whereas

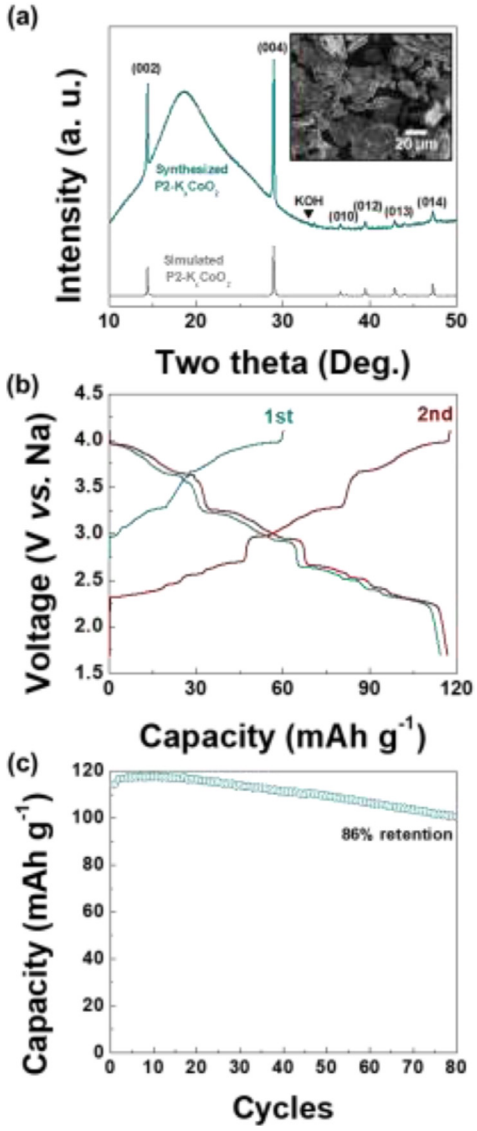

Fig. 1. (a) XRD pattern of P2-type K_xCoO_2 synthesized by a solid-state method (Inset: SEM image). (b) Charge–discharge profiles and (c) cycling stability of P2-type K_xCoO_2 in a Na half-cell.

the specific capacity of P2-type K_xCoO_2 ($x = 0.6$) is slightly lower than that of its Na analogue. This result can likely be attributed to the much larger particle size and heavier weight of P2-type K_xCoO_2 than that of its Na analogue (Figure S1a–b). Two interesting results were observed: (1) The open-circuit voltage of P2-type K_xCoO_2 after the cell assembly was much higher than that of its Na counterpart, which might be due to the different chemical potential of K_xCoO_2 ($x = 0.6$) *vs.* Na_xCoO_2 ($x = 0.74$) (*vs.* Na metal) resulting from the different alkali-ion concentration. (2) P2-type K_xCoO_2 shows a much smoother voltage profile with less obvious plateaus during the first charging process than P2-type Na_xCoO_2 although the particle size of K_xCoO_2 is larger than that of its Na analogue and, in general, the extraction of larger K ions leads to more obvious voltage steps [34–36]. The first charging profile of P2-type K_xCoO_2 in a Na cell is even smoother than that in a K cell in our previous work [37]. This phenomenon could be attributed to some degree of chemical K^+/Na^+ exchange occurring spontaneously along with the charging process, which will be further discussed in a later section. In the cycling stability test, P2-type K_xCoO_2 maintains ~86% of the specific capacity after 80 cycles, as shown in Fig. 1c.

3.2. Structure evolution during electrochemical ion-exchange reactions

To better understand the electrochemical K^+/Na^+ exchange reaction mechanisms in P2-type K_xCoO_2, we leveraged an *operando* technique using a customized electrochemistry–XRD cell, of which the charge–discharge profiles are presented in Fig. 2a along with the XRD patterns as a function of charging and discharging states in Fig. 2b. The *operando* cell delivers a capacity of ~82 mAh g^{-1} for the first charge and ~150 mAh g^{-1} for the first discharge, which is higher than the specific capacities obtained from a coin-cell configuration. The higher capacity of an *operando* cell could be due to the lower applied current rate and larger amount of electrolytes used. Interestingly, two peaks were observed at ~6.2° and ~7.1°, which are the characteristic peaks of the K-rich phase (larger d spacing, denoted by red dotted line in Figs. 2b–c) and Na-rich phase (smaller d spacing, denoted by green dotted line in Figs. 2b–d), respectively, as shown in Fig. 2b–c even before the charging process had begun, indicating that there is some degree of spontaneous K^+/Na^+ exchange. We could not differentiate the K and Na contents from the specific capacity because the chemical K^+/Na^+ exchange occurs simultaneously with the electrochemical process. During charging, the peak at 6.2° (for the K-rich phase) shifts to lower angles, which is indicative of K extraction. At the same time, the peak at 7.1° (for the Na-rich phase) moves to lower angles; however, surprisingly, its peak intensity increases and peak becomes sharper. The shift of the peak position to lower angles of the Na-rich phase indicates that the Na concentration in the layered structure is reduced. In contrast, the increase in peak intensity and peak sharpening indicate that the domain size of the Na-rich phase grows. This discrepancy signifies that there is a spontaneous K^+/Na^+ exchange reaction, which is chemically driven, even during charging. The Na concentration in the nominal composition of Na_xCoO_2 decreases to meet the equilibrium state as the voltage increases during charging; however, the domain size of Na_xCoO_2 becomes larger because K ions are replaced by Na ions. (K-rich domains become Na-rich domains). When the charging time reaches ~20 h (charging capacity: ~40 mAh g^{-1}), where a large voltage jump from 3.27 to 3.67 V occurs, the XRD peak of the K-rich phase suddenly disappears and a new XRD peak at ~6.5° evolves. Given that the peak position is between the K-rich and Na-rich phases, we suspect that the new peak corresponds to a new phase where K and Na ions are mixed. Further charging process does not change the position nor the intensity of this new XRD peak. However, the peak of the Na-rich phase shifts to lower angles, indicating Na extraction from the layered structure, until the charging time reaches ~36 h (charging capacity: ~72 mAh g^{-1}). Further charging results in a shift of the peak of the Na-rich phase to higher angles. This result indicates that the slab spacing is reduced because a large amount of Na ions is removed from the structure, which is often observed in Na layered oxides [38–40]. Upon discharging, the XRD peak evolutions appear to reverse (Fig. 2c–d). For example, the peak of the Na-rich phase shifts to lower angles until the discharge capacity is ~10 mAh g^{-1}, and then, it moves to higher angles. In addition, the XRD peak of the Na/K mixed phase at ~6.5° disappears when a large voltage step appears in the discharge profile. At the end of the discharge, a small peak of the K-rich phase at ~6.1° evolves, as shown in Fig. 2e. This demonstrates that K ions remain in the layered structure after an electrochemical K^+/Na^+ exchange cycle. The second charging process follows the same reaction trend of the first charging process (Fig. 2e) except for the peak-intensity reduction of the K-rich phase because many of K ions are exchanged with Na ions. For comparison, we also monitored the phase evolutions of Na_xCoO_2 during charging and discharging (Figure S2). No K-rich or Na/K mixed phase was observed. Notably, we observed a new peak evolution at ~7.25°, indicating a two-phase reaction region, at the end of discharging, whereas no such two-phase region was observed in the Na-rich phase at the end of discharging in the K_xCoO_2 case.

We further investigated the chemical K^+/Na^+ exchange in K_xCoO_2 using *ex situ* XRD because a spontaneous ion exchange between K and Na ions was observed in our *operando* system, as shown in Fig. 2b.

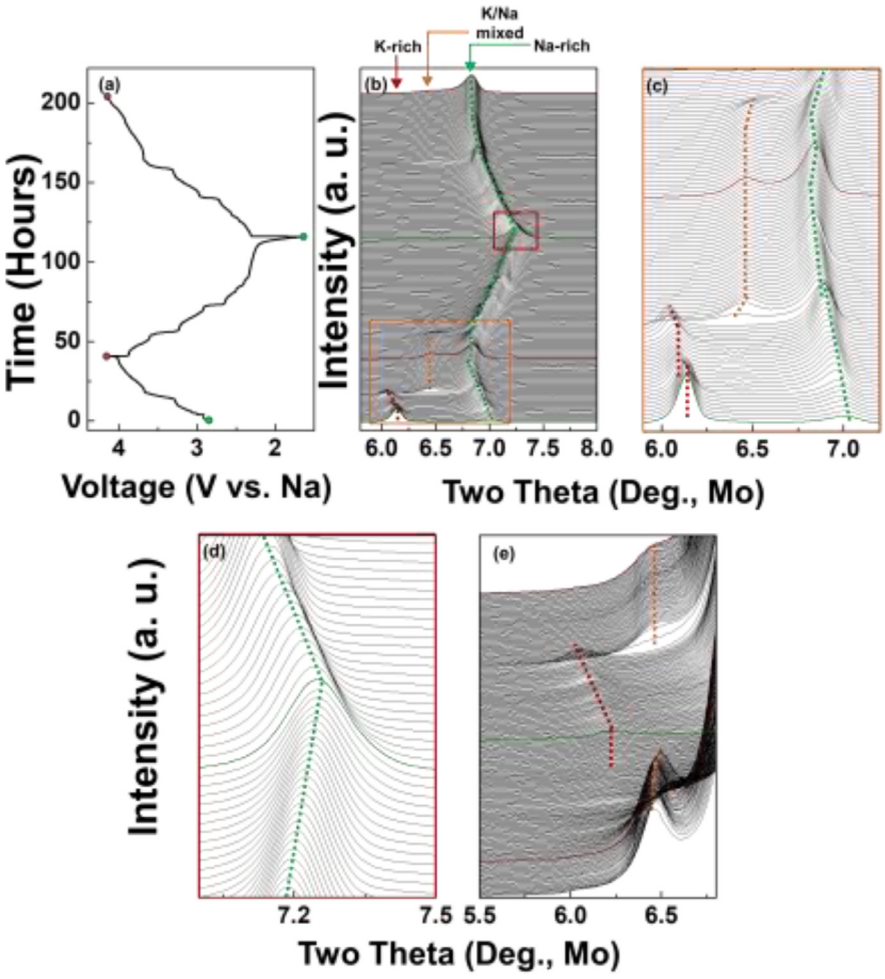

Fig. 2. Structure evolution of P2-type K_xCoO_2 during K- to Na-ion exchange. *Operando* XRD characterization results of P2-type K_xCoO_2 in a Na half-cell. (a) Charge–discharge profiles of an *operando* cell. (b) *Operando* XRD patterns of P2-type K_xCoO_2 during electrochemical K- to Na-ion exchange reactions. The brown and green lines are the XRD patterns at the end of charging and discharging, respectively. (c) Magnified regions of orange box area in (b). (d) Magnified regions of red box area in (b). (e) Magnified regions of shoulder peaks (5.5°–6.8°).

Fig. 3a presents the *ex situ* XRD patterns of P2-type K_xCoO_2 stored in 1 M $NaPF_6$ in EC/DEC electrolyte at room temperature with varied reaction time. An XRD peak of the Na-layered phase (Na_xCoO_2) begins to appear at 16° even after 2 s of reaction. The peak intensity of Na_xCoO_2 increases with increasing reaction time, and P2-type K_xCoO_2 is completely transformed into the Na phase after 48 h, which indicating the spontaneous ion exchange reaction is time-dependent. The very broad bump in Fig. 3a originates from the Kapton tape used for sealing the *ex situ* samples to avoid air exposure. A similar spontaneous ion-exchange behavior between two distinct mobile ions was also observed in the Na layered oxide $Na_{2/3}(Ni_{0.25}Mn_{0.75})O_2$ [41]. To further understand whether it is only Na ions intercalated in the K_xCoO_2 in the initial stage of ion exchange, we have monitored the peak intensity as a function of reaction time during the chemical ion exchange as shown in Fig. 3a-b. During the initial 60 s, the peak intensity of K-rich phase decreases and that of Na-rich phase increases. This demonstrates that K ions are exchanged with Na ions. We also traced the valence state of Co in K_xCoO_2 during the spontaneous ion exchange process. Fig. 3c shows the XPS analysis results of K_xCoO_2 during the ion exchange. There is no noticeable change in oxidation state of Co. Because XPS technique is surface sensitive only, we also employed XAS, which can provide bulk information (Fig. 3d-e). Overall shape of the Co K-edge X-ray absorption near edge spectroscopy (XANES) spectra does not change significantly during the spontaneous ion exchange. We have looked at the peak top energy of the Co K-edge XANES spectra, which is sensitive to the oxidation state of Co [42,43]. Interesting, we found that the Co ions went through reduction and oxidation. However, the overall change of the oxidation state is less than 0.1. This result indicates that the spontaneous K-to-Na ion exchange might involve some degree of unbalanced ion exchange process, but majority of the reaction is done by ion exchange rather than Na insertion only.

Table 1
Composition estimated from EDS and ICP.

	Charged (4.1 V)	Discharged (1.7 V)	Charged (4.5 V)
From EDS	$Na_{0.17}K_{0.07}CoO_2$	$Na_{0.5}K_{0.04}CoO_2$	$Na_{0.19}K_{0.024}CoO_2$
From ICP	$Na_{0.3}K_{0.18}CoO_2$	$Na_{0.95}K_{0.19}CoO_2$	$Na_{0.23}K_{0.11}CoO_2$

The composition and chemical element distribution in a particle after electrochemical ion-exchange reaction were investigated using the STEM-EDS mapping technique, as shown in Fig. 4. Interestingly, a relatively large amount of Na ions was observed after the first charge process (Fig. 4a–d). The composition of the charged sample was estimated to be $Na_{0.17}K_{0.07}CoO_2$ from the EDS analysis result. The composition of the charged sample estimated from inductively coupled plasma (ICP) method is $Na_{0.3}K_{0.18}CoO_2$. (see Table 1) For the composition estimation, only Na, K, and Co were considered, with the assumption that there was no oxygen loss due to the relatively low cut-off voltage (4.1 V *vs.* Na/Na^+). This finding clearly demonstrates that K^+/Na^+ exchange occurs spontaneously during the charging process such that some K ions are replaced by Na ions despite both alkali ions being extracted out of the host structure by the cell potential. In addition, we found that Na and K ions are uniformly distributed in a particle after the discharging process (Fig. 4e–h). The composition estimated from EDS analysis of the discharged state is $Na_{0.5}K_{0.04}CoO_2$, which is slightly lower than that estimated from the specific capacity observed in the electrochemical measurement. It is difficult to conclude the total number of Na/K in the system by using EDS only due to its accuracy limit. It is also

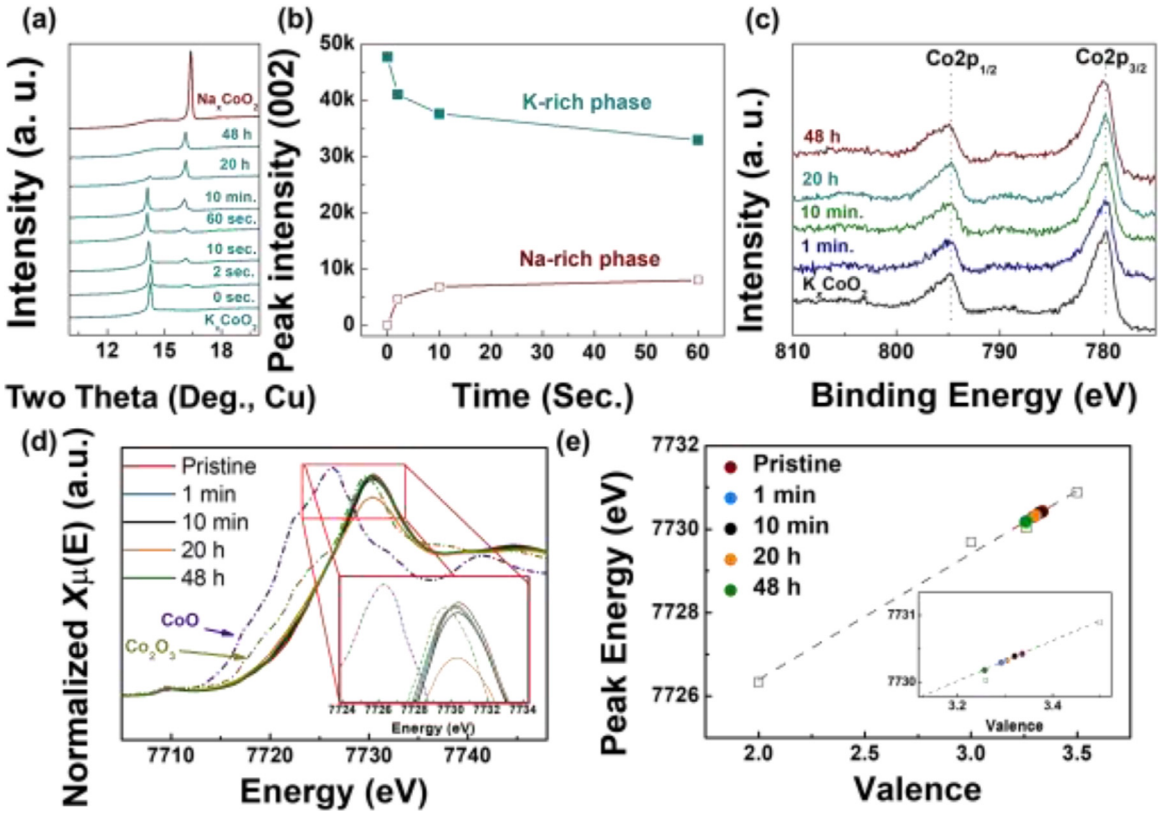

Fig. 3. (a) *Ex situ* XRD patterns of P2-type K_xCoO_2 after chemical ion exchange at room temperature with varied reaction time. (b) Peak intensity *vs*. Time plot of K-rich and Na-rich phases. (c) XPS and (d) XAS spectra of K_xCoO_2 during the spontaneous ion exchange. (e) Linear plot of valence state of Co *vs.* peak top energy of the Co K-edge XANES for quantification. For the linear plot we adopted the data points of $Na_{0.74}CoO_2$ ($Co^{3.26+}$) and $Na_{0.5}CoO_2$ ($Co^{3.5+}$) from [Ref. [44]].

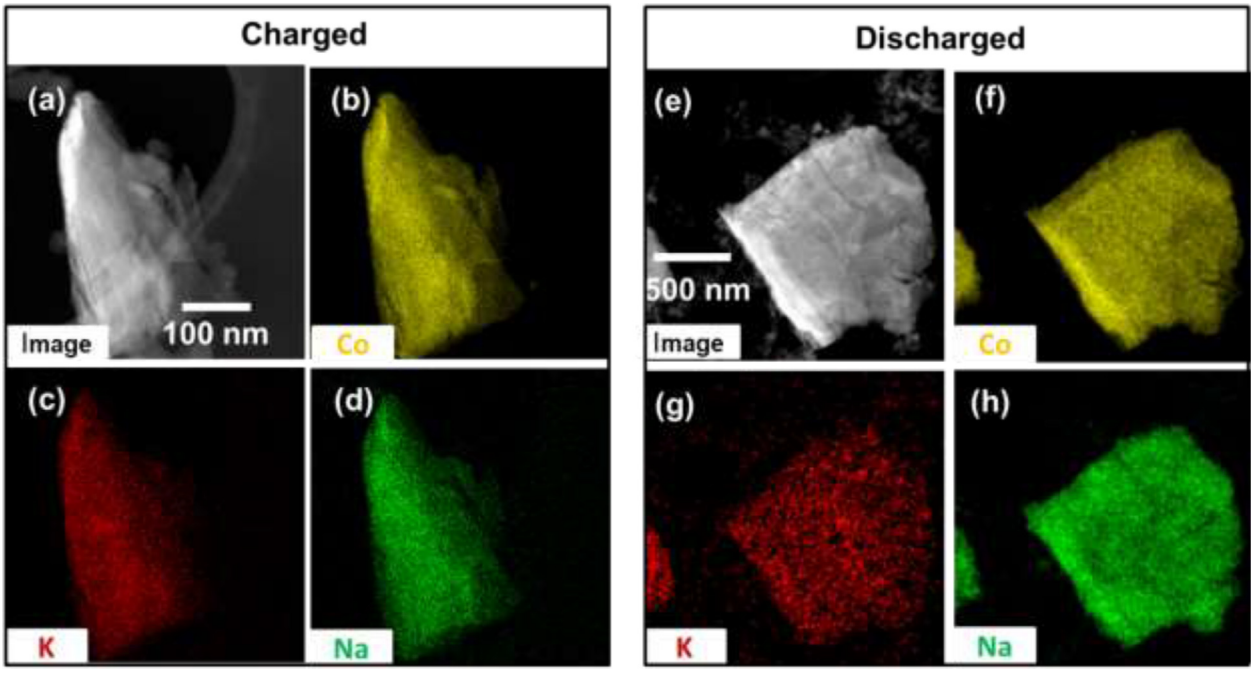

Fig. 4. (a–d) STEM–EDS results of P2-type K_xCoO_2 after the first charge. (a) STEM–HAADF image. EDS elemental maps of (b) Co, (c) K, and (d) Na. (e–h) STEM–EDS results of P2-type K_xCoO_2 after the first charge–discharge cycle. (e) STEM-HAADF image. EDS elemental maps of (f) Co, (g) K, and (h) Na.

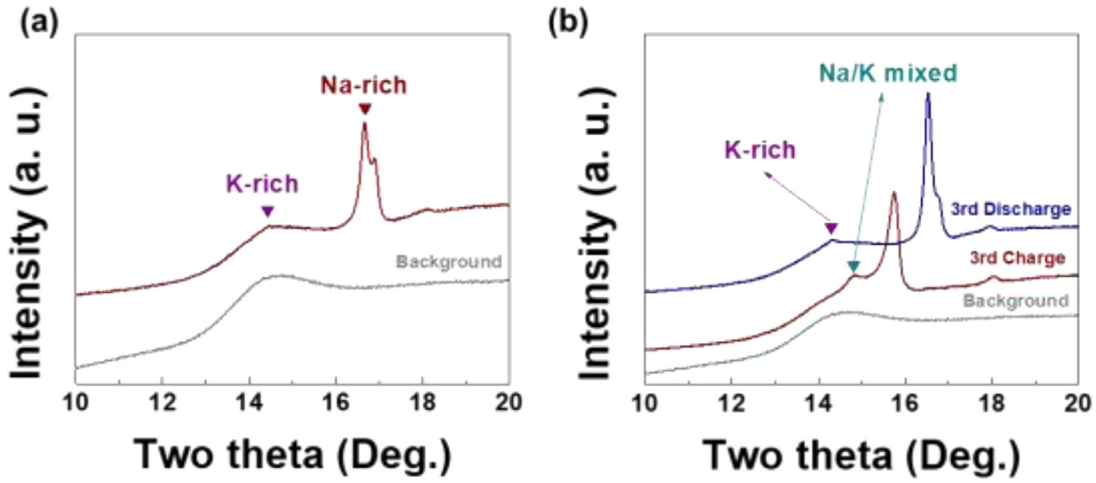

Fig. 5. ***Ex situ*** **XRD patterns of P2-type K_xCoO_2** (a) after 1 cycle of charge–discharge in a Na half-cell, followed by 20 h of chemical ion exchange, and (b) after the 3rd charge–discharge process.

possible that some level of Na and K ions would be extracted when the sample meets a trace amount of O_2 and H_2O during the TEM sampling using DEC (see experimental section), which underestimates Na and K contents. To be more accurately estimate the compositions, we used ICP method. ICP result shows much higher alkali ion concentration: $Na_{0.95}K_{0.19}CoO_2$. We do not think such high contents of Na and K ions are in the crystal structure. Excess Na and K contents likely come from solid-electrolyte interphase (SEI) formed by electrolyte decomposition and residual salts from the electrolyte. Compared to the composition of charged state above, it clearly demonstrates that the Na ions intercalate into the layered structure during the discharging. Given that there is a separation between the Na-rich and K-rich phases in XRD, where the K-rich phase has a low intensity and broad shape, it is likely that small K-rich domains form inside a large Na-rich particle. This finding is in sharp contrast to the case of Li^+/Na^+ exchange in Li_xCoO_2 and Na^+/K^+ exchange in $Na_xNi_2SbO_6$, where two distinct mobile ions are separated in distinct relatively large areas [14,27]. In our system, Na and K ions are mixed in the same structure in the charged state, as shown in Fig. 2c and 2e. During the Na intercalation (discharging), K ions want to build a separate K-rich domain but cannot travel a long distance because the diffusivity of K ions in the layered oxide structure is lower than that of Na ions [45]. Therefore, small K-rich domains can form inside a large Na-rich domain.

3.3. Residual K ions in ion-exchanged structure

We also conducted *ex situ* experiments to determine if the residual K ions are extractable after a few charge–discharge cycles. Fig. 5a presents the *ex situ* XRD pattern of P2-type K_xCoO_2 after 1 cycle in a Na half-cell, followed by 20 h of chemical ion exchange in 1 M $NaPF_6$ in EC/DEC. Similar to the *operando* experiments, a broad peak of the K-rich phase was observed at ~14.5° as well as a relatively sharp Na-rich phase at ~16.8° Unfortunately, the K-rich peak is overlapped with the background as shown in Fig. 5. However, we could highlight that there is a little peak at ~14.4 °, which belongs to K-rich layered structure by comparing the XRD pattern of background: the curvature at ~14.4 ° is different between the two. This demonstrates that the residual K ions are unlikely to be extractable or exchangeable with Na ions, unlike the pure chemical ion-exchange process (Fig. 3a). The difference in the peak positions between the *operando* and *ex situ* XRD results originate from the different X-ray sources (Mo for *in situ vs*. Cu for *ex situ*). In our *ex situ* experiments, we observed peak splitting of the Na-rich phase in contrast to the *operando* result (Fig. 2d). It is likely that such peak splitting occurs during the relaxation, which is unavoidable in the *ex situ* sample preparation process. Fig. 5b presents XRD patterns of P2-type K_xCoO_2 after the 3rd charge–discharge cycles. Notably, K-rich and intermediate (Na/K mixed) phases are maintained even after 3 cycles, again indicating that the residual K ions are not extractable.

To understand the role of residual K ions in battery performance, we compared the cycling stability of P2-type K_xCoO_2 and Na_xCoO_2 in a Na cell at 5 mA g^{-1}, as shown in Fig. 6. We used the same electrode formulation for both: 70 wt% of active material, 20 wt% of carbon, 10 wt% of PTFE binder. P2-type K_xCoO_2 exhibits 86% capacity retention after 80 cycles, whereas P2-type Na_xCoO_2 shows 65% capacity retention. We have also conducted cycling stability at a relatively high current rate (20 mA g^{-1}) as shown in Figure S3. While the specific capacity of K_xCoO_2 is lower than Na-analogue, it shows improved cycling stability (~71% retention after 140 cycles at 20 mA g^{-1}) compared to Na-version (~62% retention after 140 cycles at 20 mA g^{-1}). We also conducted elemental analysis of the K_xCoO_2 electrode after 80 cycles using TEM-EDS technique (Figure S4). The composition estimated from EDS is $Na_{0.76}K_{0.079}CoO_2$. These results clearly demonstrate that there are residual K ions in the ion exchanged layered oxide even after 80 cycles of charging-discharging process. These results indicate that the residual K ions in the Na- layered oxide have a positive effect on the cycling performance, which will be discussed in the following section. In the rate capability test (Fig. 6c-d), K_xCoO_2 shows relatively fast capacity decay as the current rate increases compared to Na_xCoO_2. This might come from the larger particle size of K_xCoO_2 than Na-analogue. Also, there could be a detrimental effect of residual K ion in the diffusion of Na ions through the layered structure.

4. Discussion

We observed that the residual K ions in the layered K_xCoO_2 after the electrochemical ion-exchange process are not replaced by Na when the sample is soaked in a Na-based solvent (1 M $NaPF_6$ in EC/DEC) for 20-h extensive chemical ion-exchange reaction (Fig. 5a). In addition, the residual K ions remain in the layered structure even after repeated electrochemical charge–discharge (ion-exchange) cycles, as shown in Fig. 5b and Figure S4. In contrast, in the pure chemical ion-exchange case, where P2-type K_xCoO_2 was stored in the Na-based solvent, the K ions were completely replaced by Na ions (Fig. 3a). These results suggest that the reaction path of the electrochemical ion-exchange process might differ from that of the chemical route. In the electrochemical ion-exchange system, we extract one mobile ion from the structure followed by the insertion of another mobile ion. In the charged state, the remaining K and/or Na ions form an ordering with vacancies to minimize the electrostatic repulsion and stabilize the structure. Therefore, the residual ion cannot be completely replaced by another ion or, at least, a very

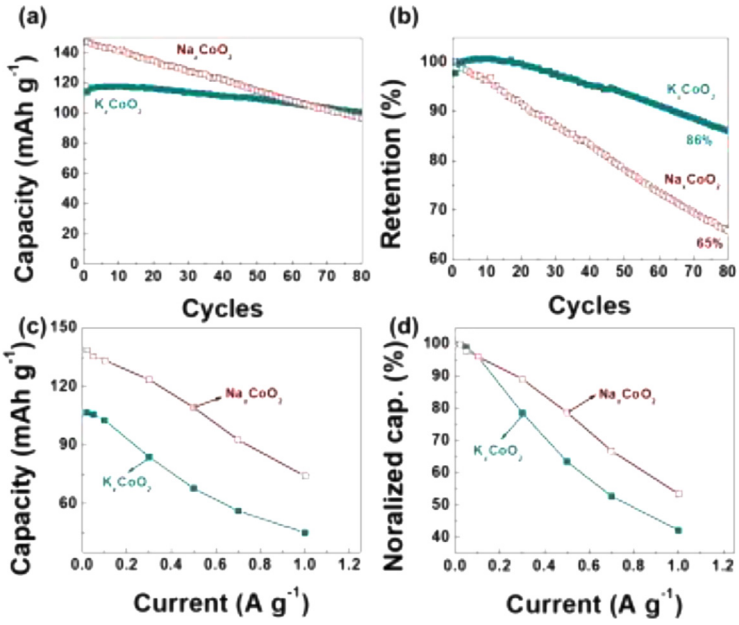

Fig. 6. (a-b) Cycle stability of P2-type K_xCoO_2 and Na_xCoO_2 in a Na half-cell at 5 mA g^{-1}. (a) Cycle number *vs.* Capacity. (b) Cycle number *vs.* Capacity retention. (c-d) Rate capability of K_xCoO_2 and Na_xCoO_2.

large number of charge–discharge cycles is required to complete the ion exchange [13,14]. To understand if more K ions can be extracted at higher voltage cut-off, we charged K_xCoO_2 up to 4.5 V (*vs.* Na/Na^+). However, it shows a significantly higher capacity than the theoretical one (140 mAh g^{-1}), given that all K ions are extracted from $K_{0.6}CoO_2$ (Figure S5). This demonstrates that there is a severe electrolyte decomposition reaction at high voltage region. TEM-EDS technique in Figure S5b shows that there are remaining K and Na ions in the structure even after the charging up to 4.5 V (*vs.* Na/Na^+). The estimated composition from the EDS is $Na_{0.19}K_{0.024}CoO_2$. Compared to the result obtained at 4.1 V (*vs.* Na/Na^+), the cathode has less K ions, indicating some degree of K ions are extracted at > 4.1 V (*vs.* Na/Na^+), but they are not completely extractable. Similarly, we could observe remaining K ions in the cathode film at 4.5 V with ICP method. The composition estimated from ICP is $Na_{0.23}K_{0.11}CoO_2$. Table 1 summarizes the composition estimated from EDS and ICP.

It is likely that the residual K ions play a positive role in improving the cycle life of the layered oxide cathode. In our electrochemical test, we found that P2-type K_xCoO_2 has better cycling stability (86% retention) than its Na analogue, as shown in Fig. 6a-b. In fact, a recent study by Wang et al. demonstrates that the introduction of K ions into the Na-layered oxides improves the capacity retention because K ions serve as pillars and prevent the structure degradation during repeated battery cycling [28]. Similarly, Tosun et al. showed that the cycling stability of $Na_{0.6}Mn_{0.35}Fe_{0.35}Co_{0.3}O_2$ can be improved by K doping [46]. In this respect, the layered oxides with Na- and K-ion mixing could be an interesting chemical space to explore for stable Na cathodes.

In our work, we discovered that K ions are spontaneously exchanged with Na ions when P2-type K_xCoO_2 is stored in 1 M $NaPF_6$ in EC/DEC (Fig. 3a). Similar behavior has also been observed in $Na_{2/3}(Ni_{0.25}Mn_{0.75})O_2$, where Na ions are replaced by Li ions with no external electric bias [41]. However, Na ions are not spontaneously replaced by K ions when P2-type Na_xCoO_2 is stored in 0.7 M KPF_6 in EC/DEC (Figure S1c). This behavior can be explained by the difference in the energetics of the layered oxide structure with Na and K ions. It is well known that the working voltage of K layered oxides is much lower than that of its Na analogues despite the lower standard redox potential of K/K^+ *vs.* Na/Na^+ [33,34,47]. In addition, our previous work demonstrates that K ions are not stable in the layered structure at high concentrations; therefore, most stoichiometric $KTMO_2$ (TM=transition metal) compounds are not thermodynamically stable except for $KCrO_2$ [48]. All of these findings indicate that K ions are less stable than Na ions

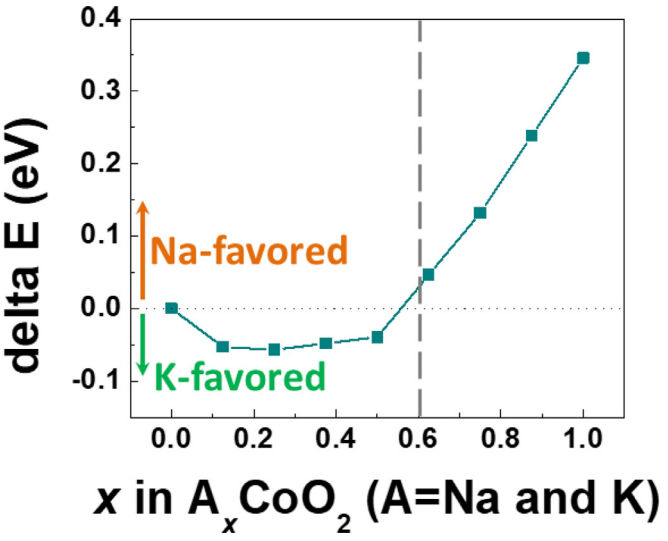

Fig. 7. Energy difference between Na_xCoO_2 and K_xCoO_2 as a function of alkali ion concentrations.

in the layered structure, resulting in a preferential K-to-Na ion replacement but not *vice versa*. We conducted DFT calculations to understand the thermodynamic driving force for the spontaneous ion exchange between K and Na in the P2-type layered oxides. Fig. 7 shows the computed energy difference between P2-type K_xCoO_2 and P2-type Na_xCoO_2 as a function of alkali ion concentrations. In a relatively low alkali ion concentration ($x < 0.5$), K ions are favored to intercalate into the layered structure. However, at a higher alkali ion concentration, Na ions are favored to insert to the layered framework. In our ion exchange system, the composition of our sample is $K_{0.6}CoO_2$. Therefore, Na would favor to be exchanged with K ions in the K_xCoO_2. This computation indicates that a spontaneous K-to-Na ion exchange would not occur if the starting material has lower K concentration (x) than 0.5 in K_xCoO_2.

Summary

In this work, the electrochemical K-to-Na ion-exchange reaction mechanisms occurring in K_xCoO_2, a representative layered oxide cathode, as a model system were investigated using operando and *ex situ*

structure characterization (XRD and TEM) techniques. Interestingly, some level of K ions remains in the layered structure despite several charge–discharge cycles. In the discharged state, K ions are preferentially separated from the Na-rich phases. In contrast, they form an intermediate phase where K and Na ions are mixed at the top of the charge. The intermediate phase formation in the charged state, where K and/or Na ions form an ordering with vacancies to minimize the electrostatic repulsion and stabilize the structure, likely prevents K ions from being completely exchanged with Na ions. Instead, we found that the residual K ions prevent the collapse of the layered structure in the high-voltage regime, improving the cycling stability.

Declaration of Competing Interest

The authors declare no conflicts of interests.

CRediT authorship contribution statement

Haegyeom Kim: Conceptualization, Supervision, Funding acquisition, Investigation, Writing – original draft, Writing – review & editing. **Young-Woon Byeon:** Investigation, Visualization, Formal analysis, Writing – review & editing. **Jingyang Wang:** Investigation, Visualization, Formal analysis, Writing – review & editing. **Yaqian Zhang:** Investigation, Formal analysis, Writing – review & editing. **Mary C. Scott:** Visualization, Supervision, Writing – review & editing. **KyuJung Jun:** Investigation, Formal analysis, Writing – review & editing. **Zijian Cai:** Investigation, Visualization, Validation, Writing – review & editing. **Yingzhi Sun:** Investigation, Writing – review & editing.

Acknowledgments

This work was supported in part by previous breakthroughs obtained through the Laboratory Directed Research and Development Program of Lawrence Berkeley National Laboratory under U.S. Department of Energy Contract No. DE-AC02-05CH11231. Work at the Molecular Foundry was supported by the Office of Science, Office of Basic Energy Sciences, of the U.S. Department of Energy under Contract No. DE-AC02-05CH11231. This research used resources of the Advanced Photon Source, an Office of Science User Facility operated for the U.S. Department of Energy, Office of Science by Argonne National Laboratory, and is supported by the U.S. Department of Energy under contract no. DE-AC02-06CH11357.

Supplementary materials

Supplementary material associated with this article can be found, in the online version, at doi:10.1016/j.ensm.2022.01.057.

References

[1] A. Clearfield, Chem. Rev. 88 (1988) 125–148, doi:10.1021/cr00083a007.
[2] C. Delmas, J.-J. Braconnier, P. Hagenmuller, Mater. Res. Bull. 17 (1982) 117–123, doi:10.1016/0025-5408(82)90192-1.
[3] A.R. Armstrong, P.G. Bruce, Nature 381 (1996) 499–500, doi:10.1038/381499a0.
[4] F. Capitaine, P. Gravereau, C. Delmas, Solid State Ionics 89 (1996) 197–202, doi:10.1016/0167-2738(96)00369-4.
[5] K. Kang, Y.S. Meng, J. Bréger, C.P. Grey, G. Ceder, Science 311 (2006) 977–980, doi:10.1126/science.1122152.
[6] A.D. Robertson, A.R. Armstrong, A.J. Fowkes, P.G. Bruce, J. Mater. Chem. 11 (2001) 113–118, doi:10.1039/B002948N.
[7] A.R. Armstrong, A.D. Robertson, R. Gitzendanner, P.G. Bruce, J. Solid State Chem. 145 (1999) 549–556, doi:10.1006/jssc.1999.8216.
[8] D. Eum, B. Kim, S.J. Kim, H. Park, J. Wu, S.-P. Cho, G. Yoon, M.H. Lee, S.-K. Jung, W. Yang, W.M. Seong, K. Ku, O. Tamwattana, S.K. Park, I. Hwang, K. Kang, Nat. Mater. 19 (2020) 419–427, doi:10.1038/s41563-019-0572-4.
[9] X. Cao, H. Li, Y. Qiao, M. Jia, P. He, J. Cabana, H. Zhou, Energy Storage Mater. 38 (2021) 1–8, doi:10.1016/j.ensm.2021.02.047.
[10] Z. Yang, J. Zhong, J. Feng, J. Li, F. Kang, Adv. Funct. Mater. 31 (2021) 2103594, doi:10.1002/adfm.202103594.
[11] S. Baskar, K. Sada, P. Barpanda, ECS Trans. 80 (2017) 357–364, doi:10.1149/08010.0357ecst.
[12] K. Sada, B. Senthilkumar, P. Barpanda, Chem. Commun. 53 (2017) 8588–8591, doi:10.1039/C7CC02791E.
[13] N. Naveen, W.B. Park, S.C. Han, S.P. Singh, Y.H. Jung, D. Ahn, K.-S. Sohn, M. Pyo, Chem. Mater. 30 (2018) 2049–2057, doi:10.1021/acs.chemmater.7b05329.
[14] H. Kim, D.-H. Kwon, J.C. Kim, B. Ouyang, H. Kim, J. Yang, G. Ceder, Chem. Mater. 32 (2020) 4312–4323, doi:10.1021/acs.chemmater.0c01152.
[15] M.G.T. Nathan, W.B. Park, N. Naveen, S. Park, K.-S. Sohn, M. Pyo, J. Electrochem. Soc. 167 (2020) 100507, doi:10.1149/1945-7111/ab9568.
[16] H. Park, W. Ko, Y. Lee, J. Kang, J. Ahn, J.-K. Yoo, J. Kim, J. Mater. Chem. A 9 (2021) 11802–11811, doi:10.1039/D1TA02247D.
[17] J. Kang, H. Park, W. Ko, Y. Lee, J. Ahn, J.-K. Yoo, S.H. Song, H. Kim, J. Kim, J. Mater. Chem. A 9 (2021) 9898–9908, doi:10.1039/D1TA01602D.
[18] X. Lin, J. Huang, H. Tan, J. Huang, B. Zhang, Energy Storage Mater. 16 (2019) 97–101, doi:10.1016/j.ensm.2018.04.026.
[19] J.S. Ko, P.P. Paul, G. Wan, N. Seitzman, R.H. DeBlock, B.S. Dunn, M.F. Toney, J.Nelson Weker, Chem. Mater. 32 (2020) 3028–3035, doi:10.1021/acs.chemmater.0c00004.
[20] G. Li, Z. Yang, Y. Jiang, C. Jin, W. Huang, X. Ding, Y. Huang, Nano Energy 25 (2016) 211–217, doi:10.1016/j.nanoen.2016.04.051.
[21] B. Jeon, J.W. Heo, J. Hyoung, H.H. Kwak, D.M. Lee, S.-T. Hong, Chem. Mater. 32 (2020) 8772–8780, doi:10.1021/acs.chemmater.0c01112.
[22] S. Kim, L. Yin, M.H. Lee, P. Parajuli, L. Blanc, T.T. Fister, H. Park, B.J. Kwon, B.J. Ingram, P. Zapol, R.F. Klie, K. Kang, L.F. Nazar, S.H. Lapidus, J.T. Vaughey, ACS Energy Lett. 5 (2020) 3203–3211, doi:10.1021/acsenergylett.0c01663.
[23] Z.-L. Xu, J. Park, J. Wang, H. Moon, G. Yoon, J. Lim, Y.-J. Ko, S.-P. Cho, S.-Y. Lee, K. Kang, Nat. Commun. 12 (2021) 3369, doi:10.1038/s41467-021-23703-x.
[24] J.M. Paulsen, C.L. Thomas, J.R. Dahn, J. Electrochem. Soc. 146 (1999) 3560–3565, doi:10.1149/1.1392514.
[25] B. Xiao, K. Wang, G.-L. Xu, J. Song, Z. Chen, K. Amine, D. Reed, M. Sui, V. Sprenkle, Y. Ren, P. Yan, X. Li, Adv. Mater. 31 (2019) 1805889, doi:10.1002/adma.201805889.
[26] H. Gwon, S.-W. Kim, Y.-U. Park, J. Hong, G. Ceder, S. Jeon, K. Kang, Inorg. Chem. 53 (2014) 8083–8087, doi:10.1021/ic501069x.
[27] C. Heubner, B. Matthey, T. Lein, F. Wolke, T. Liebmann, C. Lämmel, M. Schneider, M. Herrmann, A. Michaelis, Energy Storage Mater. 27 (2020) 377–386, doi:10.1016/j.ensm.2020.02.012.
[28] Y. Wang, Z. Feng, P. Cui, W. Zhu, Y. Gong, M.-A. Girard, G. Lajoie, J. Trottier, Q. Zhang, L. Gu, Y. Wang, W. Zuo, Y. Yang, J.B. Goodenough, K. Zaghib, Nat. Commun. 12 (2021) 13, doi:10.1038/s41467-020-20169-1.
[29] B. Ravel, M. Newville, J. Synchrotron Rad. 12 (2005) 537–541, doi:10.1107/S0909049505012719.
[30] P.E. Blöchl, Phys. Rev. B 50 (1994) 17953–17979, doi:10.1103/PhysRevB.50.17953.
[31] G. Kresse, J. Furthmüller, Phys. Rev. B 54 (1996) 11169–11186, doi:10.1103/PhysRevB.54.11169.
[32] S.P. Ong, W.D. Richards, A. Jain, G. Hautier, M. Kocher, S. Cholia, D. Gunter, V.L. Chevrier, K.A. Persson, G. Ceder, Comput. Mater. Sci. 68 (2013) 314–319, doi:10.1016/j.commatsci.2012.10.028.
[33] A. Jain, G. Hautier, S.P. Ong, C.J. Moore, C.C. Fischer, K.A. Persson, G. Ceder, Phys. Rev. B 84 (2011) 045115, doi:10.1103/PhysRevB.84.045115.
[34] H. Kim, H. Ji, J. Wang, G. Ceder, Trends Chem. 1 (2019) 682–692, doi:10.1016/j.trechm.2019.04.007.
[35] Y. Tian, G. Zeng, A. Rutt, T. Shi, H. Kim, J. Wang, J. Koettgen, Y. Sun, B. Ouyang, T. Chen, Z. Lun, Z. Rong, K. Persson, G. Ceder, Chem. Rev. 121 (2021) 1623–1669, doi:10.1021/acs.chemrev.0c00767.
[36] Y. Hironaka, K. Kubota, S. Komaba, Chem. Commun. 53 (2017) 3693–3696, doi:10.1039/C7CC00806F.
[37] H. Kim, J.C. Kim, S.-H. Bo, T. Shi, D.-H. Kwon, G. Ceder, Adv. Energy Mater. 7 (2017) 1700098, doi:10.1002/aenm.201700098.
[38] J.W. Somerville, A. Sobkowiak, N. Tapia-Ruiz, J. Billaud, J.G. Lozano, R.A. House, L.C. Gallington, T. Ericsson, L. Häggström, M.R. Roberts, U. Maitra, P.G. Bruce, Energy Environ. Sci. 12 (2019) 2223–2232, doi:10.1039/C8EE02991A.
[39] J.C. Kim, D.-H. Kwon, J.H. Yang, H. Kim, S.-H. Bo, L. Wu, H. Kim, D.-H. Seo, T. Shi, J. Wang, Y. Zhu, G. Ceder, Adv. Energy Mater. 10 (2020) 2001151, doi:10.1002/aenm.202001151.
[40] J. Yang, A.E. Maughan, G. Teeter, B.J. Tremolet de Villers, S.-M. Bak, S.-D. Han, ChemSusChem 13 (2020) 5972–5982, doi:10.1002/cssc.202001963.
[41] W. Hua, S. Wang, K. Wang, A. Missyul, Q. Fu, M.S. Dewi Darma, H. Li, V. Baran, L. Liu, C. Kübel, J.R. Binder, M. Knapp, H. Ehrenberg, S. Indris, Chem. Mater. 33 (2021) 5606–5617, doi:10.1021/acs.chemmater.1c00962.
[42] M. Fakkao, K. Chiba, Y. Kimura, T. Nakamura, T. Okumura, K. Nitta, Y. Terada, Y. Uchimoto, K. Amezawa, J. Ceram. Soc. Jpn. 125 (2017) 299–302, doi:10.2109/jcersj2.16253.
[43] T. Okumura, Y. Yamaguchi, M. Shikano, H. Kobayashi, J. Mater. Chem. 22 (2012) 17340–17348, doi:10.1039/C2JM32024J.
[44] V.V. Poltavets, M. Croft, M. Greenblatt, Phys. Rev. B 74 (2006) 125103, doi:10.1103/PhysRevB.74.125103.
[45] H. Kim, D.-H. Seo, J.C. Kim, S.-H. Bo, L. Liu, T. Shi, G. Ceder, Adv. Mater. 29 (2017) 1702480, doi:10.1002/adma.201702480.
[46] S.G. Tosun, D. Uzun, S. Yeşilot, J. Solid State Electrochem. 25 (2021) 1271–1281, doi:10.1007/s10008-021-04906-0.
[47] W. Lee, J. Kim, S. Yun, W. Choi, H. Kim, W.-S. Yoon, Energy Environ. Sci. 13 (2020) 4406–4449, doi:10.1039/D0EE01277G.
[48] H. Kim, D.-H. Seo, A. Urban, J. Lee, D.-H. Kwon, S.-H. Bo, T. Shi, J.K. Papp, B.D. McCloskey, G. Ceder, Chem. Mater. 30 (2018) 6532–6539, doi:10.1021/acs.chemmater.8b03228.